Instrument Science Report WFC3 2001-017

Modeling the impact of ghosts in WFC3/UVIS

Massimo Stiavelli, STScI,
Joseph Sullivan and John Fleming,
BATC
July 30, 2001

Abstract

This ISR briefly describes the various ghosts expected to be present in WFC3 UVIS, including their location, intensity, and potential science impact. Four of the 19 WFC3 UVIS ghosts do not satisfy the CEI Spec. However, their science impact is less serious than that of four ghosts due to reflections between the camera head windows which – due to their compactness - have relatively high surface brightness despite being within instrument specifications.

1. Introduction

It is common for imagers, especially with off-axis optics, to display for bright stars in the field of view additional – usually out of focus – images produced by two or more internal reflections between the detector and refractive elements in the optical chain. The UVIS channel of WFC3 is characterized by 3 refractive elements (2 windows in the CCD camera head plus the filter) for a total of 7 surfaces (2 each for the refractive elements plus the detector). Any pair of these surfaces can in principle produce a ghost image. The total maximum number of two-reflection ghosts will thus be 21. Higher order ghosts requiring four or more reflections will be much weaker than the double reflection ghosts and will be ignored in this analysis.

The location of these surfaces is dictated purely by geometric optics, their intensity by the reflectivity of the optics. In Section 2 we will discuss the various ghosts that will be seen in WFC3 UVIS. The intensity of these ghosts and a number of possible options for the window coatings will be discussed in Section 3. Our conclusions are presented in Section 4.

2. The UVIS channel ghosts

At a purely qualitative level we expect WFC3 UVIS to show three main classes of ghosts. A first class is that of ghosts produced by reflection within the two surfaces of individual refractive elements. The total number of these ghosts will be three and their location will be very close to that of the primary image since the two faces of each refractive element are parallel and the distance between the two surfaces is small. Due to the small difference in optical path these ghosts are those with the smallest angular size (Figure 2).

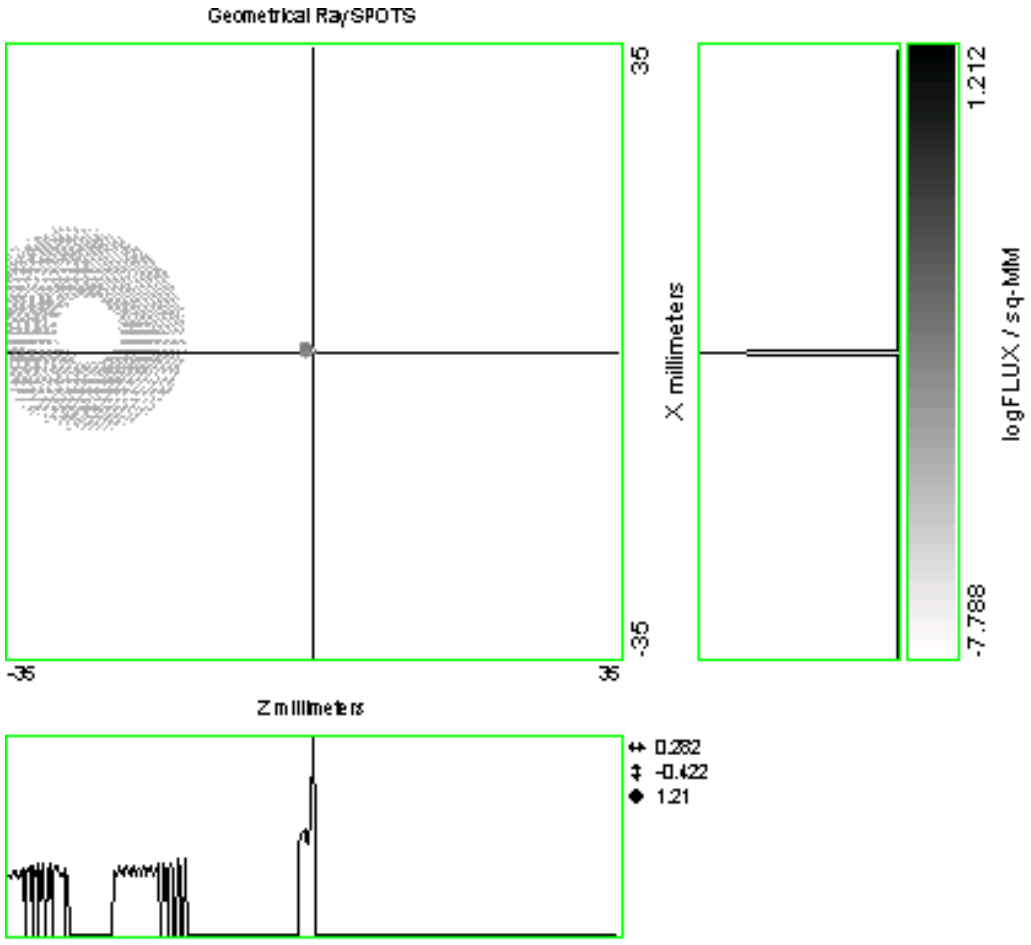

Figure 1 : layout of the camera ghost for a source at the center of the field of view. Visible are 15 ghosts in two groups. The highest surface brightness ghosts are the three produced by internal reflections within individual refractive and the four produced by reflections between the two windows. The (eight) diffuse ghosts are due to window-filter reflections.

A second kind of ghost, is produced by the internal reflections in the camera head between the windows and the detector. Since each surface contributes with a ghost, the two windows produce a total of 4 ghosts. We expect these ghosts to be out of focus and offset from

the primary image by a large angle since there is a ~20 degree angle between the windows and the CCD detector. The relative angle also makes the ghost path shorter on one corner of the field of view compared to the others. Thus ghosts will have smaller apparent size and smaller separation from the source for sources on the corner of the field of view with the minimum ghost path. They become progressively larger and more separated as the distance of the source from this corner increases (see Figure 3).

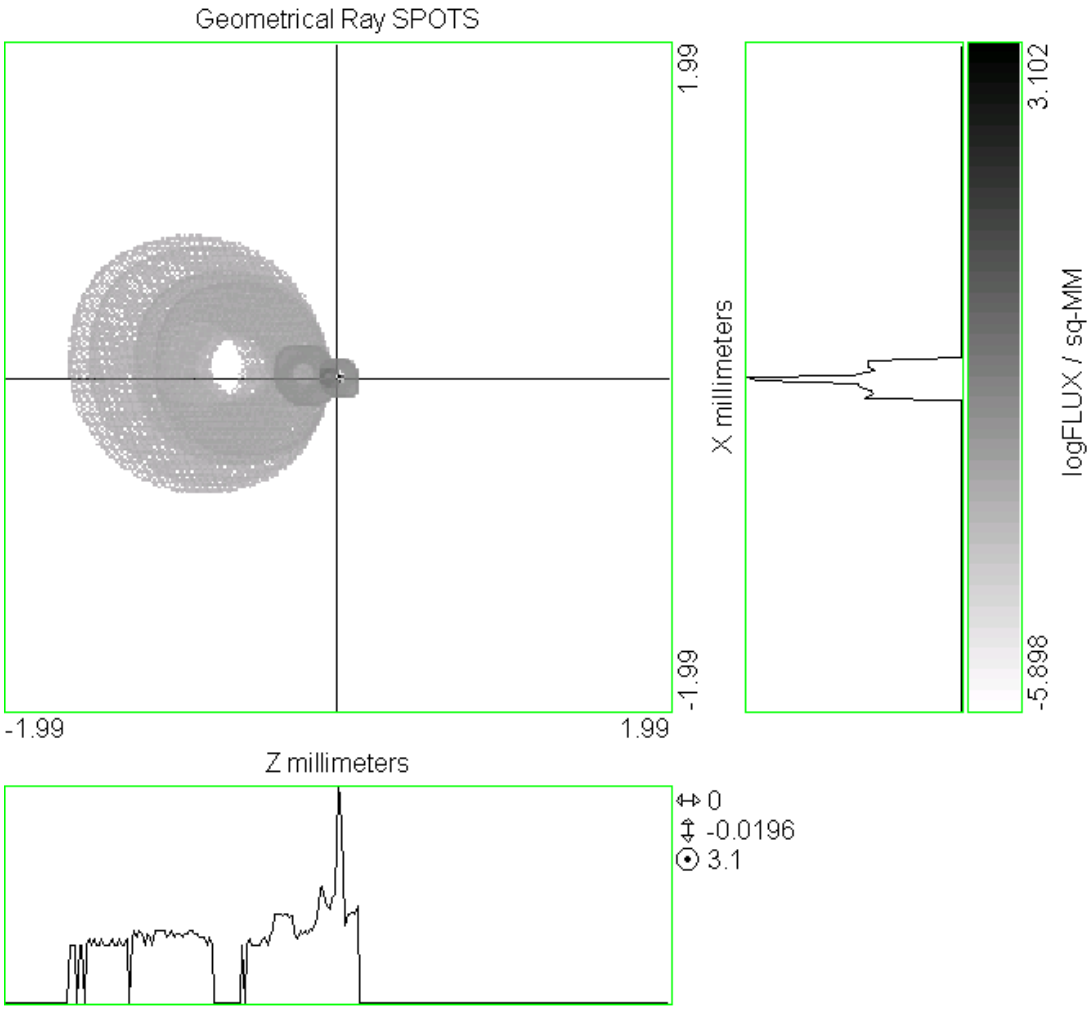

Figure 2 : zoom on the central 7 ghosts for the same configuration as in Figure 1. Visible are two group of ghosts. The highest surface brightness ghosts are the three produced by internal reflections within individual refractive elements. The filter-filter ghost is almost perfectly aligned.. The four ghosts produce by the reflections between the two camera head windows are individually visible.

Finally, there will be a number of ghosts produced by reflections involving larger path differences, e.g., those between the inner and the outer window or those between one of the windows and the filter. These ghosts will be of very large angular size since the ghost will be far from focus. A maximum of 14 of such ghosts could exist.

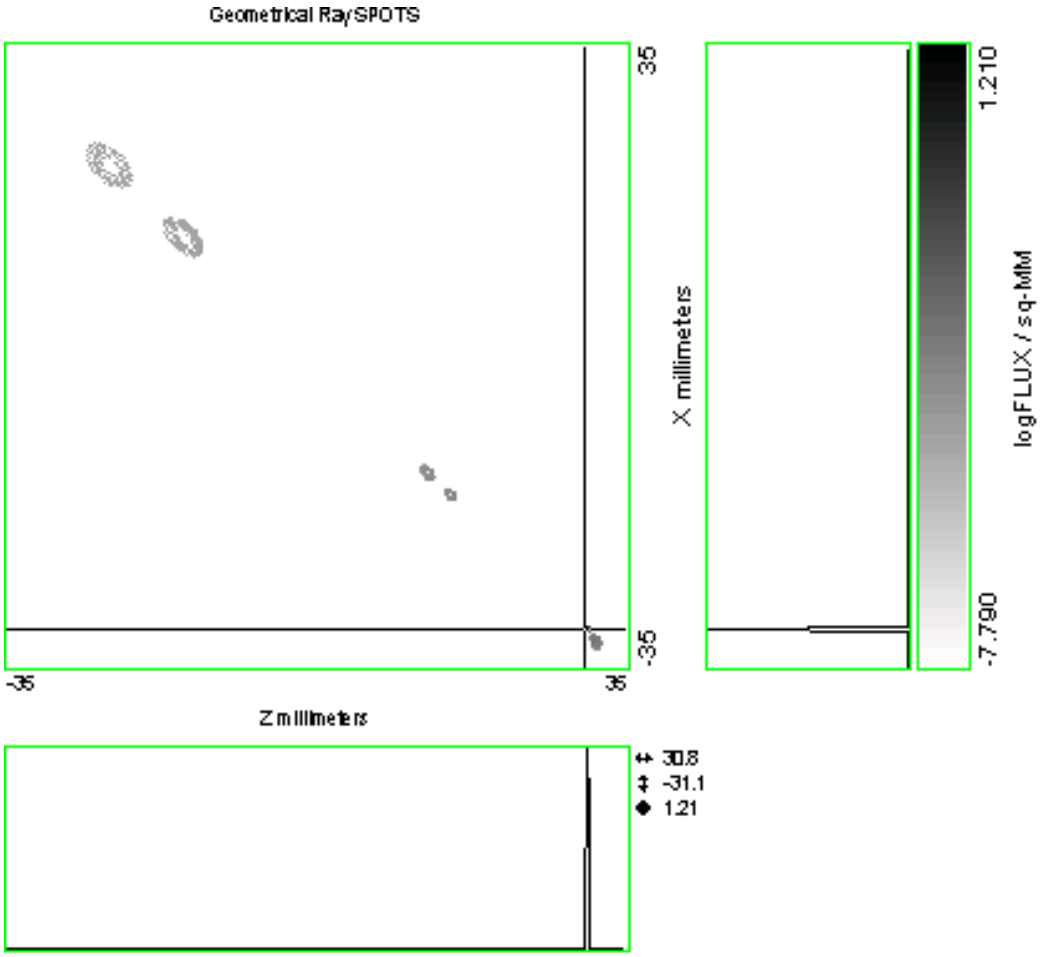

Figure 3 : Configuration of the 4 window-detector ghosts visible when the source is at the corner of the field of view. The filter ghost is also visible.

In order to analyze these ghosts more quantitatively, we have used two independent approaches. One of the authors (JF) performed a ghost analysis using ASAP software from Breault Research Organization. The Code V model uvspider_f.len (see BASD SER OPT-044 by Jennifer Turner-Valle) was imported into ASAP. Geometric global coordinate ray traces were performed in both Code V and ASAP to ensure that the model was properly converted to ASAP. Then baffles and masks were added to the optical model based on information provided by Ball mechanical engineers. The model does not include the telescope spiders. This will have no effect on the relative power in the ghosts and image, but the appearance of the

ghosts does not show the spider obscurations. Two ghost reflections were enabled for the analysis.

Unless otherwise stated, the figures herein were generated using ASAP and run at 633 nm. The model predictions for the relative power in the ghost to the image show excellent agreement with hand calculations, so the relative power results could easily be converted to different wavelengths or be changed based on different reflectivity data. Different wavelengths will not cause significant changes in the size of the ghosts.

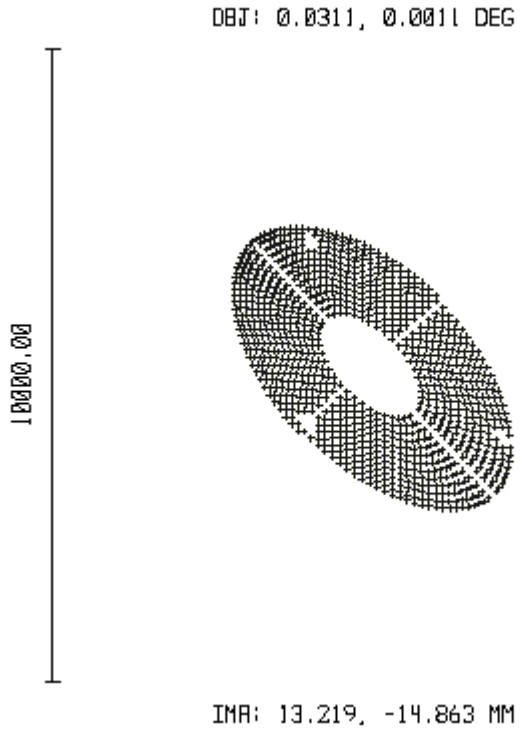

Figure 4 : ZEMAX image of the ghost produced by the reflections off the detector and the inner surface of the outer window. The scale is in μm. Note the obscuration due to the spiders and the primary mirror pads. This ghost is the second on the left in Figure 3.

Another author (MS) has carried out a similar analysis using ZEMAX EE 10.0. The ZEMAX software can be used to carry out a ghost analysis either by using non-sequential components or by using the ghost focus analysis tool for a sequential system. The former option cannot easily be used for WFC3 due to a limitation in the ZEMAX software, namely, the non-sequential component automatic translation does not support non-standard surfaces like the anamorphic aspheres represented by M1 and M2. The sequential ghost focus analysis is also limited in that it does not support coordinate breaks, which are essential for describing an off-axis system. The work around was to produce intermediate files for each double reflection and edit them when needed in order to add the required coordinate breaks by hand (usually two of them). The ZEMAX analysis includes the effect of the spider (which are visible in the ghost images, see Figure 4). The fact that the main conclusions agree with the ASAP analysis confirms that spiders do not play a significant role.

The two analyses produce results in very good agreement and are consistent with the qualitative analysis above. The total effective number of ghosts present is 19 since the two

detector-filter ghosts do not fall on the detector. The maximum number of ghosts seen for an individual stellar image is 17. The actual number depends critically on the location of the source within the field of view. In Figures 1, 2 and 3 we show three representative cases from the ASAP analysis.

We have found that the ghost position depends on wavelength with typical displacements ranging from less than a pixel to 10-60 pixels for the detector-window ghosts.

Table 1 : ghost intensities at 250 nm and 633 nm for the UV optimized (left columns), B band optimized (central columns) and a V band optimized (right columns) window coating.

Path description	**UV optimized**		**B band optimized**		**V band optimized**	
	250 nm	633 nm	250 nm	633 nm	250 nm	633 nm
	(%)	(%)	(%)	(%)	(%)	(%)
Filter front to filter back	0.010	0.010	0.010	0.010	0.010	0.010
Inner window front to back	0.040	0.078	0.078	0.043	0.168	0.036
Outer window front to back	0.040	0.078	0.078	0.053	0.168	0.036
Detector to inner window back	**0.280**	**0.860**	**0.392**	**0.706**	**0.574**	**0.583**
Detector to inner window front	**0.269**	**0.812**	**0.370**	**0.674**	**0.528**	**0.561**
Detector to outer window back	**0.258**	**0.767**	**0.350**	**0.643**	**0.485**	**0.540**
Detector to outer window front	**0.248**	**0.725**	**0.331**	**0.614**	**0.447**	**0.520**
Outer window front to filter back	0.020	0.028	0.028	0.023	0.041	0.019
Outer window front to filter front	0.010	0.026	0.014	0.022	0.020	0.018
Outer window back to filter back	0.019	0.026	0.026	0.021	0.036	0.018
Outer window back to filter front	0.009	0.024	0.013	0.020	0.018	0.017
Inner window front to outer window back	0.040	0.078	0.078	0.053	0.168	0.036
Inner window front to outer window front	0.038	0.074	0.074	0.050	0.155	0.035
Inner window back to outer window back	0.038	0.074	0.074	0.050	0.142	0.035
Inner window back to outer window front	0.037	0.070	0.070	0.048	0.142	0.033
Inner window front to filter back	0.018	0.025	0.025	0.021	0.035	0.018
Inner window front to filter front	0.009	0.024	0.012	0.020	0.017	0.017
Inner window back to filter back	0.018	0.024	0.024	0.020	0.032	0.017
Inner window back to filter front	0.009	0.022	0.012	0.019	0.016	0.016
Windows Throughput	**0.922**	**0.893**	**0.893**	**0.911**	**0.832**	**0.960**

3. Intensity of the individual ghosts

Once the locations of the various ghosts are identified, it is a simple to compute their intensity once the reflectivity of the various surfaces is known. We have assumed a reflectivity of 0.01 for the filter and the measured reflectivity for a blue-optimized EEV-Marconi CCD - which is close to 30 per cent in the visible.

Table 2 : ghost intensities and sizes at 633 nm. For the detector-window ghost they have been computed assuming a UV band optimized window coating.

Path description	**% of primary image**	**Ghost radius (mm)**
Filter front to filter back	0.010	0.12
Inner window front to back	0.078	0.06
Outer window front to back	0.078	0.18
Detector to inner window back	0.860	2.1
Detector to inner window front	0.812	2.2
Detector to outer window back	0.767	2.8
Detector to outer window front	0.725	3.2
Outer window front to filter back	0.028	10.9
Outer window front to filter front	0.026	11.0
Outer window back to filter back	0.026	11.1
Outer window back to filter front	0.024	11.2
Inner window front to outer window back	0.078	0.52
Inner window front to outer window front	0.074	0.71
Inner window back to outer window back	0.074	0.58
Inner window back to outer window front	0.070	0.76
Inner window front to filter back	0.025	11.6
Inner window front to filter front	0.024	11.7
Inner window back to filter back	0.024	11.6
Inner window back to filter front	0.022	11.7

A typical reflectivity for the window coating is shown in Figure 5. Due to the relatively large wavelength range required for the UVIS channel, potential AR coating suppliers are finding it difficult to achieve better than 2% to 4% reflectivity per surface over the entire range from 180 nm to 1050nm. Although lower reflectivity values (0.5% to 1.5%) can be achieved at selected short wavelength intervals, the consequence is getting much higher reflectivity values (as high as 8 % to 12 %) at either end of the UVIS wavelength range. A simple single layer MgF_2 coating optimized for 400 nm (B band optimized) provides the most uniform performance over the entire wavelength range (see Figure 5). MgF_2 coatings are relatively low risk and robust to implement. Alternative possibilities would be single layer MgF_2 coatings optimized for 280 nm (UV optimized) or 510 nm (V band optimized). A UV-optimized coating decreases the UV ghosts while increasing the visible ones (see Table 1). Regardless of the coating option, the four ghosts involving reflections off the detector do not satisfy the WFC3

CEI Spec 4.3.2.6.1 specifying that individual ghost intensities have to be below 0.2 per cent. The remaining 15 components satisfy the Specs. The various choices of coatings also imply different window throughputs. However, the instrument will satisfy CEI Specs on throughput regardless of the choice for the window coating. The V-band optimized coating brings the four out of spec ghosts to the same intensity while keeping the others within specs. The UV optimized coating has the maximum UV throughput. In the following we will assume that this is the adopted coating (see Table 2).

The total energy in the ghosts generated by internal reflections of the refractive components is 0.17 per cent. The 12 ghosts generated by reflections off different components not including the detector contribute a total of 0.6 per cent, spread over a large area, so that the average flux per pixel within the ghost is $6.0\ 10^{-7}$ of the source intensity. This implies that in F606W a star with magnitude V=17.2 will produce in a full orbit a ghost with intensity of 4 e/pixel. However, the same star in the primary image will have reached ~100 times the full well capacity of the detector. Note also that this average flux is a pessimistic estimate since the 12 individual ghosts will not exactly overlap one another.

Finally, the individual detector-window ghosts have relative intensity per pixel in the range $1.5\ 10^{-7}$ to $7.5\ 10^{-8}$. They will become visible at the 4 e/pixel level in full orbit F606W exposures for stars in the magnitude range 15.7 to 14.6. Once again such stars will be heavily saturated.

Note that 8 of the 12 diffuse ghosts are due to reflections involving the filter. They will presumably be stronger than described above for the narrow band filters.

As we stated previously, the four detector-window ghosts do not satisfy our CEI Specs. However, those due to the outer camera head window will fall on the field of view only when the source is close to one of the corners, covering about 9.2 per cent of the field of view. The remaining two ghosts will appear in roughly 27.9 per cent of the field of view.

We have also investigated the presence of ghost images from sources outside the field of view and found none. This suggests that for typical sources outside the FOV the instrument is well baffled.

4. Conclusions

The UVIS channel of WFC3 is characterized by a significant number of ghosts generated by the selected filter (we do not allow observation with multiple filters), the two camera head windows and the detector. We have adopted in our analysis a UV optimized coating for the camera head windows. Up to 17 individual ghosts will appear for an individual star. For the broad band filters, all of these ghosts will have a brightness per pixel much below 1 electron for non-saturated stars and therefore we expect that they will not be significantly affect the science of the camera. Of these ghosts, the 4 generated by reflections between the two camera head windows and the 4 generated by reflections of the camera head windows with the detector are compact enough to appear above the noise level in multiple orbit integrations with broad band filters of heavily saturated (~100-1000 times the full well) stars. The four window-window ghosts individually satisfy our CEI Spec while the four detector-window ghosts do not. However, the science impact of the four window-window ghost is probably higher: their smaller size gives them roughly the same surface brightness of the more intense detector-window ghosts and they will appear over most of the field of view in contrast to the detector-window ghosts that are only visible on a small fraction of the field.

It would be possible to change the optical design by increasing the tilt angle between detector and CCD window and thus completely eliminating the four out of spec ghosts. We do not recommend this strategy because:

i) The detector-window ghosts are not those with the most serious science impact,

ii) 70 per cent of the field does not contain these ghosts,

iii) increasing the window-detector tilt would have undesirable impact on the UV PSF and possibly on other aspects of the instrument.

Finally, the issue arises of whether the filter placement can be optimized to minimize the impact of ghosts. In particular, the narrow band filters may be characterized by the worst ghosts (due to their higher reflectivity) and it may be appropriate to mount these filters the closest to the detector so as to minimize the size of the filter-filter ghost.

5. Acknowledgements

We thank John MacKenty and Massimo Robberto for useful comments.

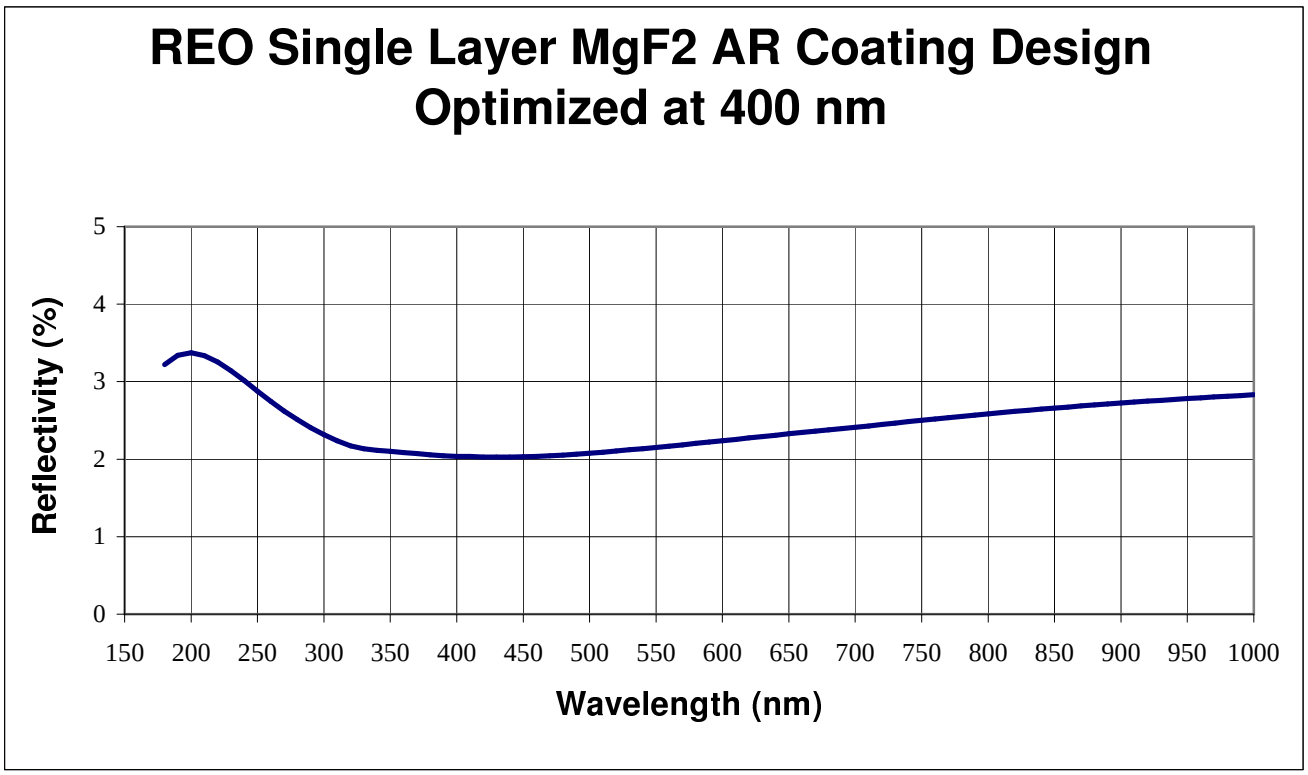

Figure 5 : example of reflectivity as a function of wavelength for a single layer MgF_2 camera head window coating optimized for 400 nm (B band optimized). It is very difficult to design a coating with uniformly low reflectivity over the whole wavelength range from 2000 A to 10000 A.